The Two-Domain NK1 Fragment of Plasminogen: Folding, Ligand Binding, and Thermal Stability Profile†

Justin T. Douglas,‡,§ Priska D. von Haller,‡,||,⊥ Marion Gehrmann,§ Miguel Llinás,*,§ and Johann Schaller||

Department of Chemistry, Carnegie Mellon University, 4400 Fifth Avenue, Pittsburgh, Pennsylvania 15213, and Department of Chemistry and Biochemistry, University of Berne, Freiestrasse 3, CH-3012 Berne, Switzerland

Received December 10, 2001

ABSTRACT: The two-domain fragment N+K1 (rNK1) [Glu^1−Glu^{163}] of human plasminogen was expressed in *E. coli* as a hexahistidine-tagged fusion protein and chromatographically purified. The ^{1}H NMR spectrum supports proper folding of the K1 component within the refolded rNK1 construct (rNK1/K1). The functional properties of rNK1/K1 were investigated via intrinsic fluorescence titration with kringle-specific ω-aminocarboxylic acid ligands. The affinities closely match those previously measured for the isolated K1, which indicates that the N-domain does not significantly affect the interaction of ligands with the lysine binding site of K1. Far-UV CD spectra recorded for the N-domain suggest conformational plasticity and flexibility for the module. Two classes of spectra, referred to as types A and B, were identified with the type A spectrum reflecting a higher secondary structure content than that estimated for the type B spectrum. Subtracting the CD spectrum of rK1 from that of rNK1 yields a spectrum (Δ) which reflects the conformation of the N-domain within the rNK1 construct (rNK1/N). Δ resembles the type A spectrum, suggesting that rNK1/N adopts a relatively more ordered conformation, stabilized by the adjacent rNK1/K1 domain. In contrast, thermal unfolding curves determined via CD indicate that the rNK1/N slightly lowers the melting temperature (T_m) of rNK1/K1. Independence of the two domains within rNK1 was tested by monitoring the thermal unfolding of rNK1/K1 when in the presence of the kringle-specific ligand AMCHA, which left the rNK1/N T_m essentially unaffected, while increasing that of the rNK1/K1 by ∼10 °C.

Plasminogen (Pgn),[1] the precursor of the serine protease plasmin (Pln), the main component of the fibrinolytic system, is a mosaic structure consisting of an N-terminal domain, five in-tandem kringle repeats, and a C-terminal, trypsin-like, serine protease module. Kallikrein, tissue-type plasminogen activator, and urokinase-type plasminogen activator proteolytically cleave Pgn at the Arg^{561}−Val^{562} peptide bond, thus activating the catalytic unit. Subsequent self-proteolysis leads to release of the N-terminal peptide [Glu^1−Lys^{77}], henceforth referred to as the N-domain. Thus, the N-domain effectively constitutes the pro-peptide of Pgn.

Removal of the N-domain from the intact Glu^1-Pgn results in a less compactly folded structure for Lys^{78}-Pgn, as measured by alterations in its hydrodynamic properties (*1*). This structural change may be correlated with an increased conversion of Pgn to Pln by plasminogen activators (*2*). Since ^{1}H NMR experiments show that the N-terminal cyanogen bromide fragment of the N-domain [Glu^1−HSer^{57}] (CB-NTP) binds to rK1, rK2, K4, and K5 (*3*, *4*), the closed conformation probably results from intramolecular interactions between the N-domain and one or more kringles. Therefore, it is not surprising that 6-aminohexanoic acid (6-AHA), via competitive interaction with the kringles, increases the radius of gyration of Glu^1-Pgn by inducing an open conformation of the protein (*5*). Thus, interactions between the N-domain and one or more kringles are likely to influence the global fold and activity of Pgn (*6*).

† These studies were supported by Swiss National Science Foundation Grants 31-45816.95 and 31-52236.97 and by NIH Grant HL-29409.

* Corresponding author. Phone: 412 268 3130, Fax: 412 268 1061, E-mail: llinas@andrew.cmu.edu.

‡ These authors contributed equally to this work.

§ Carnegie Mellon University.

|| University of Berne.

⊥ Present address: Institute for Systems Biology, 4225 Roosevelt Way NE, STE 200, Seattle, WA 98105.

[1] Abbreviations: 5-APA, 5-aminopentanoic acid; 6-AHA, 6-aminohexanoic acid; 7-AHA, 7-aminoheptanoic acid; AMCHA, *trans*-(aminomethyl)-cyclohexanecarboxylic acid; BASA, *p*-benzylaminesulfonic acid; BNPS-skatole, 2-(2-nitrophenylsulfenyl)-3-methyl-3-bromoindolenine; CB-NTP, N-terminal cyanogen bromide cleaved fragment of Pgn N-domain [Glu^1−HSer^{57}]; CD, circular dichroism; Δ, difference CD spectrum obtained by subtracting the spectrum of rK1 from that of rNK1; $\Delta\epsilon$, differential extinction coefficient for left and right circularly polarized light; ΔH^{vH}, van't Hoff enthalphy; ΔS^{vH}, van't Hoff entropy; DSC, differential scanning calorimetry; EK, enterokinase; ESI-MS, electrospray ionization mass spectrometry; HGF, hepatocyte growth factor; His-tag, peptide MRGSH$_6$GSD$_4$K; K1, kringle 1 [Cys^{84}−Cys^{162}]; rK1, recombinant kringle 1; K2, kringle 2 [Cys^{166}−Cys^{243}]; rK2, recombinant kringle 2; K3, kringle 3 [Cys^{256}−Cys^{333}]; K4, kringle 4 [Cys^{358}−Cys^{435}]; K5, kringle 5 [Cys^{462}−Cys^{541}]; LBS, lysine binding site; lysine-Bio-Gel, lysine-substituted Bio-Gel P-300; N-domain, N-terminal domain [Glu^1−Lys^{77}]; rN, recombinant N-terminal domain with His-tag and Trp cleavage site; NK1, N-terminal domain + kringle 1 fragment of Pgn [Glu^1−Glu^{163}]; rNK1, recombinant N-terminal domain + kringle 1 fragment of Pgn; NK1/K1, K1 component within the refolded rNK1 construct; NK1/N, N-domain component within the refolded rNK1 construct; Ni^{2+}-NTA, Ni^{2+}-nitrilotriacetic acid; Pgn, human plasminogen; Pln, human plasmin; PRG-A, plasminogen-related gene A; PRG-B, plasminogen-related gene B; RP-HPLC, reverse-phase HPLC; TES, *N*-tris(hydroxymethyl)methyl-2-aminoethanesulfonic acid; T_m, melting temperature.

10.1021/bi016018j CCC: $22.00
Published on Web 02/16/2002

The N-domain consists of 77 amino acids and contains 2 disulfide bonds in a 1−4, 2−3 disulfide bond pattern. Similar domains with ~30% sequence identity are found in hepatocyte growth factor (HGF) and related macrophage stimulating factor (*7*, *8*). Additionally, two genes, PRG-A and PRG-B, have been identified which exhibit >90% sequence identity with the Pgn N-domain (*9*). Based on a homology search and structure prediction, the N-domain, PRG-A and PRG-B, along with the apple domain of the plasma prekallikrein family and various nematode proteins have recently been hypothesized to define a new discrete unit, called the PAN module (*10*). PRG-B gene expression has been detected in various neoplastic tissues (*11*, *12*), suggesting a possible involvement of this domain in cell growth and regulation. Further study of the intact Pgn N-terminal PAN module is required to understand both its role in Pgn conformation and activity and the structural and biological properties of the isolated domain.

Because the NK1 two-domain fragment cannot be generated proteolytically from isolated Pgn, the multidomain construct was obtained via recombinant DNA gene expression. Here we report the cloning, expression, purification, folding/thermal stability characterization, and ligand binding properties of rNK1. Proper refolding and secondary structure were assessed via ligand binding titrations, NMR spectroscopy, and circular dichroism (CD) spectroscopy. The thermal stability of the two-domain construct was also determined by CD. Since both the N and K1 subunits have also been individually expressed (*12*−*14*), as rN and rK1, respectively, comparing the spectrum of the rNK1 construct to the spectra of each module separately probes structural properties of the two-domain construct, including interdomain interactions.

EXPERIMENTAL PROCEDURES

Materials. Polyclonal goat anti-Pgn sera and alkaline phosphatase conjugate to rabbit antibodies against goat IgG were purchased from Sigma. Restriction endonucleases were obtained from Roche Diagnostics. *Taq* DNA polymerase, calf intestinal alkaline phosphatase, and T4 DNA ligase were purchased from Promega. Lysine-Bio-Gel P-300 (Bio-Rad) was prepared according to Brunisholz et al. (*15*). Ni^{2+}-nitrilotriacetic acid agarose (Ni^{2+}-NTA agarose), QIAprep Spin Miniprep Kit, and QIAquick Gel Extraction Kit were purchased from QIAGEN. Agarose and acrylamide were purchased from Bio-Rad.

Bacterial Strains and Plasmids. E. coli strain BL21 (F^- *ompT* $r_B^-m_B^-$) was used for the expression of rNK1. Plasmid pQE-8 utilized for the expression of the recombinant proteins was obtained from QIAGEN. The vector carries the *E. coli* bacteriophage T5 promotor/*lac*-operator element N250PSN250P29, a synthetic ribosomal binding site, RBSII, the transcriptional terminator t_0 of phage λ, the promoter-free gene for chloramphenicol acetyltransferase with its genuine translational signals, the transcriptional terminator T1 of the *E. coli rrn*B operon, and a β-lactamase selectable marker, and fuses an N-terminal hexahistidine tag to the recombinant protein (*16*). Plasmid pREP4, purchased from QIAGEN, expresses elevated levels of the *lac* repressor and carries the gene for neomycin phosphotransferase. Plasmid pPLGKG, kindly provided by Prof. Hedén (University of Lund, Sweden), contains the complete cDNA sequence of Pgn (*17*).

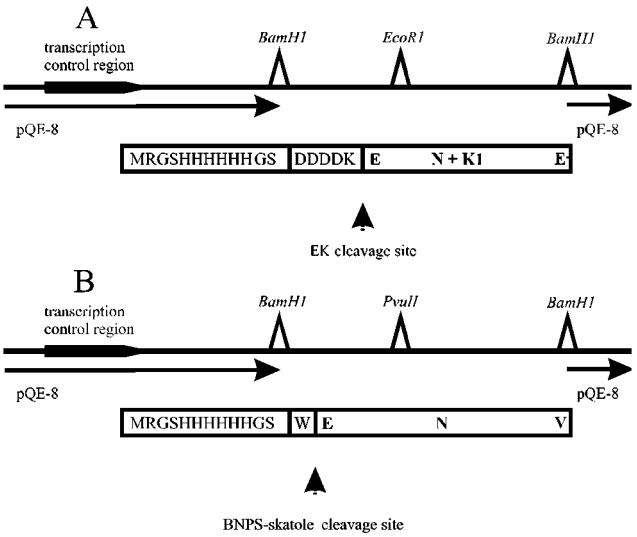

FIGURE 1: Expression vector constructs for rNK1 (A) and rN (B) in pQE-8. The indicated *Bam*HI endonuclease restriction sites, the EK recognition site (DDDDK), the BNPS-skatole cleavage site (W), and the two stop codons were introduced by the corresponding 5′- and 3′-PCR primers. Directionality of the insert was confirmed with *Eco*RI and *Pvu*II for rNK1 and rN, respectively.

DNA Manipulations. Plasmid isolations were carried out according to the QIAprep Spin Miniprep Kit manual. Synthesis of oligonucleotides and DNA sequencing were performed by Microsynth (St. Gallen, Switzerland). DNA fragments generated by restriction endonucleases were purified on 1.5% agarose gels, visualized by ethidium bromide, and recovered from the gel by the QIAquick Gel Extraction Kit according to the supplier's instructions.

Construction of the Expression Vectors for rNK1 [Glu^1−Glu^{163}]. The DNA segment of rNK1 was amplified from pPLGKG by PCR. The 5′-primer, which binds to the noncoding strand of Pgn cDNA, introduces a *Bam*HI restriction endonuclease site and a cDNA segment coding for an enterokinase (EK) recognition site upstream of the codon for Glu^1 (5′-CG *GGA TCC* GAT GAC GAT GAC AAA GAG CCT CTG GAT GAC TAT GTG-3′). The 3′-primer, complementary to a region of the coding strand, was used to introduce two **stop codons**: a *Bam*HI and a *Nde*I restriction endonuclease site after the codon for Glu^{163} (3′-CTG TAA GAA CTC ACA CTT **ATT ATC** *CCT AGG GTA TAC* TCG AG-5′).

The amplified rNK1 cDNA fragment was cloned into *Bam*HI-cleaved and dephosphorylated pQE-8 (Figure 1A) and transformed into *E. coli* strains of BL21 that already contained the repressor plasmid pREP4. To determine the direction of the insert, the plasmids formed in various clones were digested with *Eco*RI. Both strands of the insert were sequenced by the chain termination method (Microsynth, Switzerland).

Expression and Isolation of rNK1. The protocol followed is essentially that of Cleary et al. (*18*) and Marti et al. (*19*). Cells were grown at 37 °C in 2 × YT medium (100 μg of ampicillin/mL, 25 μg of kanamycin/mL) in 2 L round-bottom flasks to an OD_{600} of about 0.7−0.9. To induce the production of the recombinant proteins, isopropyl-thio-β-D-galactopyranoside was added to a final concentration of 2 mM. Cells were grown for an additional 5.5 h at 37 °C and harvested by centrifugation for 30 min (4000*g*, 4 °C). The

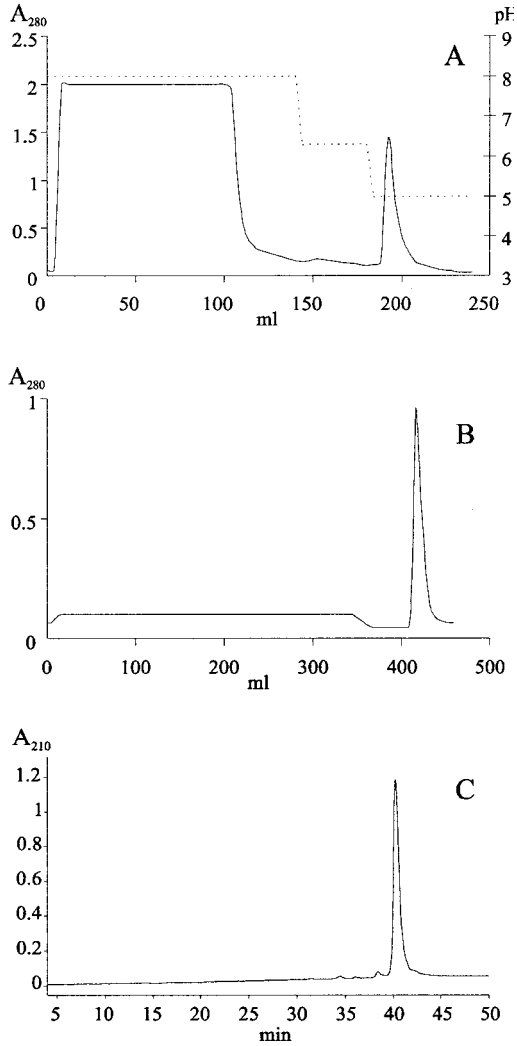

FIGURE 2: Chromatographic purification of rNK1. (A) Ni^{2+}-NTA agarose: Crude extract loaded onto a Ni^{2+}-NTA agarose column (1.5 × 4 cm) with a flow rate of 0.5 mL/min at pH 8 and eluted at pH 5. (B) Lysine-Bio-Gel: after refolding, the rNK1 was loaded onto a lysine-Bio-Gel column (1.5 × 6 cm) at a flow rate of 0.5 mL/min and eluted with 200 mM 6-AHA. (C) RP-HPLC: rNK1 analyzed on an Aquapore Butyl column (2.1 mm × 100 mm, widepore, 30 nm, 7 μm) using a linear acetonitrile gradient. The peak fraction was collected and used for further analysis.

cell paste was stored at −20 °C. The protein extracts were analyzed on 10% SDS−PAGE gels and blotted onto nitrocellulose membranes. Novel bands were detected by Ponceau S staining and were verified as domains of Pgn by an ELISA based on polyclonal antibodies against native Pgn.

For the isolation of rNK1, the cell paste was thawed and suspended in extraction buffer (6 M guanidine hydrochloride in 0.1 M sodium phosphate, pH 8; 5 mL/g of cell paste). The suspension was stirred overnight at 4 °C and centrifuged (30 min, 15000*g*, 4 °C). The supernatant was loaded onto a Ni^{2+}-NTA agarose column (1.5 × 4 cm) equilibrated with extraction buffer pH 8. After successive washes with extraction buffer pH 8 and pH 6.3, the recombinant protein was eluted from the column with extraction buffer pH 5 (Figure 2A).

Reverse-Phase (RP)-HPLC. RP-HPLC was carried out on a Hewlett-Packard liquid chromatograph 1090 using an Aquapore Butyl column (2.1 mm × 100 mm, widepore, 30 nm, 7 μm; Applied Biosystems) eluted with a linear acetonitrile gradient. Solution A, 0.1% (by volume) trifluoroacetic acid in water, and solution B, 0.1% (by volume) trifluoroacetic acid and 80% (by volume) acetonitrile in water, were used at a flow rate of 0.3 mL/min.

Refolding and Purification of rNK1. During refolding, gentle dialysis was performed to minimize partial precipitation of the protein. From earlier studies (*12*, *19*, *20*), it is known that under these conditions the disulfide bonds of kringle domains and of the N-domain pair correctly due to the strong conformational determinants which seem to be present in both structures. The pH of the effluent was adjusted to 8, and 1,4 dithio-*dl*-threitol was added to a final concentration of 5 mM. After being stirred overnight at 4 °C, the solution was slowly (6 h) added, with continuous stirring at 4 °C, to 4 volumes of 50 mM sodium phosphate buffer, pH 8, containing 1.25 mM each of reduced and oxidized glutathione. The solution was dialyzed against 50 mM sodium phosphate, pH 8, and loaded onto a column of lysine-substituted Bio-Gel P-300 (lysine-Bio-Gel, 1.5 × 5 cm). After the column was washed with loading buffer, rNK1 was eluted with 50 mM sodium phosphate, pH 8, containing 200 mM 6-AHA (Figure 2B), dialyzed against water, acidified to pH 3−4 with formic acid, and lyophilized. Refolding was monitored by RP-HPLC on an Aquapore Butyl column. The totally reduced form of rNK1 eluted at 45% B as a sharp, single peak, and the completely refolded form eluted at about 40% B while the folding intermediates appeared between. This shift might be caused by the change of the hydrophobicity on the surface of the proteins. The finally purified rNK1 eluted as a sharp, symmetrical peak upon RP-HPLC on an Aquapore Butyl column (Figure 2C). The N-terminal sequence Met-Arg-Gly-Ser-His was checked by automated Edman degradation, and the amino acid composition yielded values compatible with the protein sequence and confirmed the absence of 6-AHA.

Expression, Purification, and Refolding of rK1 and rN. rK1 was expressed, isolated, refolded, and characterized according to Marti (*14*). rN with an N-terminal hexahistidine tag and a Trp (Figure 1B) instead of a factor Xa cleavage site were expressed, purified, and refolded essentially as reported (*12*). Cleavage at the single Trp residue was carried out for 22 h at room temperature with 2-(2-nitrophenylsulfenyl)-3-methyl-3-bromoindolenine (BNPS-skatole) [1.2-fold excess (w/w) versus protein] in 60% acetic acid (by volume) and in the presence of phenol [2-fold excess (w/w) versus protein] to minimize cleavage at Tyr residues (*21*).

Characterization of rNK1. For amino acid analyses, samples were hydrolyzed in the gas phase with 6 M hydrochloric acid containing 0.1% (v/v) phenol for 24 h at 115 °C under vacuum (*22*). The liberated amino acids were caused to react with phenyl isothiocyanate, and the resulting phenylthiocarbamyl amino acids were analyzed by RP-HPLC on a Nova Pak C_{18} column (4 μm, 3.9 mm × 150 mm; Waters) in a Hewlett-Packard liquid chromatograph 1090 with an automatic injection system (*23*). The N-terminal sequence analysis was carried out in a pulsed-liquid-phase sequenator 477A from Applied Biosystems. The released amino acids were analyzed on-line according to instructions from Applied Biosystems. The mass of the recombinant proteins was determined by electrospray ionization mass spectrometry (ESI-MS) using a VG Platform instrument (Micromass).

Intrinsic Fluorescence Measurements. The effect of ω-aminocarboxylic acids on the intrinsic fluorescence of recombinant proteins was measured in 50 mM sodium phosphate, pH 8, at 25 °C on a Fluoro Max luminescence spectrophotometer (*13*). The concentration of the ligand in a 5 μM protein solution was increased in 1, 5, or 20 μM steps depending on the binding affinity of the investigated kringle in the ligand concentration range of 0−200 μM until the change of intrinsic fluorescence was constant. Fluorescence was measured at 340 nm with excitation at 298 nm. For AMCHA, the maximum intrinsic fluorescence value was determined by averaging the value of the asymptote obtained from other ligands, weighted by the error. Data were analyzed using the Levenberg−Marquardt algorithm (*24*).

Circular Dichroism Spectroscopy. Far-UV CD spectroscopic data were recorded on a Jasco J-715 spectropolarimeter equipped with a PFD 350S Peltier-type temperature controller. The spectrophotometer was calibrated with (+)-10-camphorsulfonic acid (Aldrich) (*25*). 1 mm quartz cells (Starna) were used for all experiments. Protein samples were dissolved in 10 mM TES, 50 mM NaF, pH 7.5 (*26*). Protein concentrations were estimated according to Pace (*27*), except for rN. A low extinction coefficient coupled with minimal solubility lead to overestimation of rN concentration. Empirically adjusting the concentration to minimize differences with the reported spectrum of rN (*12*) standardized the procedure. This is, however, inconsequential for qualitative screening of folding. Secondary structure content was assessed from the far-UV CD spectra using CDsstr (*28*) with seven denatured proteins included in the basis set (*29*, *30*). The difference spectrum, NK1 minus K1 (Δ hereafter), was calculated on a protein molar basis before normalization to take into account the number of residues in the difference construct.

Assuming cooperative, reversible folding for a globular protein domain, the temperature-dependent CD at a given wavelength reflects the equilibrium between folded and unfolded forms. On this basis, the equilibrium van't Hoff enthalpy (ΔH^{vH}) and entropy (ΔS^{vH}) of unfolding can be estimated from the experimental data. The melting temperature $T_m = \Delta H^{vH}/\Delta S^{vH}$ can be calculated and checked against the inflection point of the temperature-dependent dichroism profile. Thermal melting of secondary structure was monitored by CD in the far-UV region at either 222 or 198 nm. Samples were measured from 5 to 95 °C with a heating rate of 45 °C/h. Curves were nonlinearly fit to the equation (*31*)

$$y(T) = \frac{y_N(T) + y_D(T)\cdot\exp\frac{(-\Delta H^{vH} + T\Delta S^{vH})}{RT}}{1 + \exp\frac{(-\Delta H^{vH} + T\Delta S^{vH})}{RT}} \quad (1)$$

using the Levenberg−Marquardt algorithm (*24*) where $y(T)$ represents the experimental $\Delta\epsilon$ (M^{-1} cm^{-1}) at the given wavelength as a function of temperature and R the gas constant. The linear functions $y_N(T)$ and $y_D(T)$ represent the temperature-dependent contribution of native and denatured protein, respectively, to the experimental $\Delta\epsilon$ (M^{-1} cm^{-1}) at a given wavelength. Experimental errors were estimated by fitting extreme subsets of the measured data set.

Backcalculation of CD Spectra. From coordinates deposited in the Protein DataBank, percent secondary structure was estimated via xtlsstr (*32*). Far-UV CD spectra were then "backcalculated" using a secondary structure basis set generated via singular value decomposition of representative protein CD spectra, effectively reversing the algorithm for analysis of CD spectra (*28*).

RESULTS

Characterization of rN. The rN molecular mass of 10 600.5 ± 0.9 Da determined by ESI-MS concurs with 10 601.9 Da, the theoretical value for the His-tag construct with a Trp cleavage site. Amino acid and sequence analysis data are in agreement with the expected values (data not shown). The removal of the His-tag with BNPS-skatole, on a preparative scale, proved to be impractical owing to only partial cleavage of the Trp^{-1}−Glu^{1} bond and the propensity of Met^{57} and Met^{69} to oxidize to the corresponding Met-sulfoxides. Therefore, all further studies were carried out with rN containing the fusion peptide. The typical yield of rN was approximately 1.2 mg/g of wet cell pellet (4 mg/L of cell culture)

Characterization of rNK1. The rNK1 molecular mass of 20 665.8 ± 0.8 Da, determined by ESI-MS, agrees with the expected value of 20 665.8 Da for the NK1 construct. Amino acid and sequence analysis data are in agreement with the expected values (data not shown). The removal of the His-tag from rNK1 with EK was not successful because of internal cleavage sites in the hinge region between the N and K1, identified via ESI-MS and N-terminal sequence analyses to be the peptide bonds Arg^{68}−Met^{69} and Lys^{77}−Lys^{78}, which together with the Lys^{78}−Val^{79} bond are known to be accessible to Pln (*33*) and are cleaved upon activation. Therefore, all further characterizations were carried out with rNK1 bearing the N-terminal fusion tail. Dialysis of rNK1 at pH 3−4 to remove the residual 6-AHA from the affinity chromatographic purification step on lysine-Bio-Gel led to limited cleavages at the Met^{69}−Arg^{70}, Arg^{70}−Asp^{71}, Leu^{74}−Phe^{75}, and Phe^{75}−Glu^{76} peptide bonds as detected by ESI-MS and N-terminal sequence analysis. When the residual 6-AHA was removed by RP-HPLC, no such cleavages were observed.

Since the lysine affinity of rNK1 depends directly on the native three-dimensional structure of the kringle domain, binding to lysine-Bio-Gel suggests correct folding and half-cystine pairing for the K1 domain within the construct. Furthermore, the Leu^{128} (kringle Leu^{46}) $CH_3^{\delta,\delta'}$ doublet in the high-field region of the ^1H NMR spectrum of rNK1 (Figure 3), which is a signature of native kringle structure (*34*), confirms proper conformation of the kringle domain. The protein analytical data showed that the lysine affinity chromatographic step efficiently removes misfolded protein and impurities not separated during purification on Ni^{2+}-NTA agarose. The typical yield of rNK1 amounted to approximately 600 μg/g of wet cell pellet (3 mg/L of cell culture).

Ligand Binding to rNK1. Ligand-induced fluorescence response profiles are shown in Figure 4. Equilibrium association constant (K_a) values resulting from nonlinear fits of the Langmuir adsorption isotherm to the data are listed in Table 1. Linear ω-aminocarboxylic acids yielded K_a values of 51.8 ± 3.3 mM^{-1} for 5-APA, 73.7 ± 7.0 mM^{-1} for 6-AHA, and 12.4 ± 1.1 mM^{-1} for 7-AHA, and the cyclic ligands yielded values of 100.4 ± 7.7 mM^{-1} for BASA and

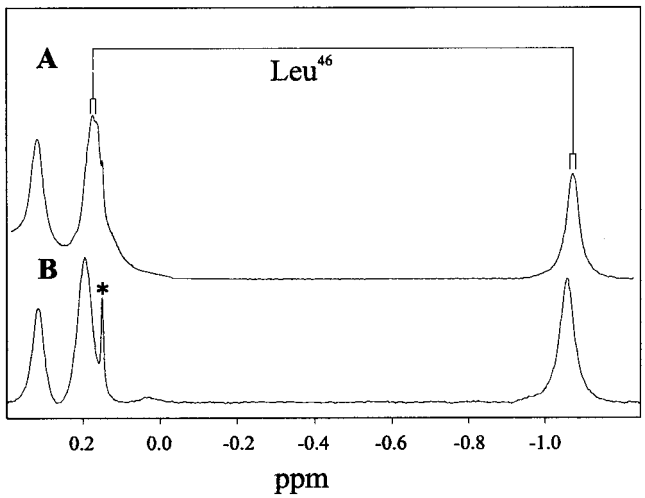

FIGURE 3: High-field region ^{1}H NMR spectra of rK1 (A) and rNK1 (B). Shifted K1 Leu^{46} methyl δ, δ' resonances are shown connected. Spectra were recorded at 500 MHz (A) and 600 MHz (B). Proteins dissolved to ~0.5 mM in ^2H_2O; spectra recorded at pH* 7.2 (A) and pH* 5.0 (B). Impurity signal denoted by an asterisk.

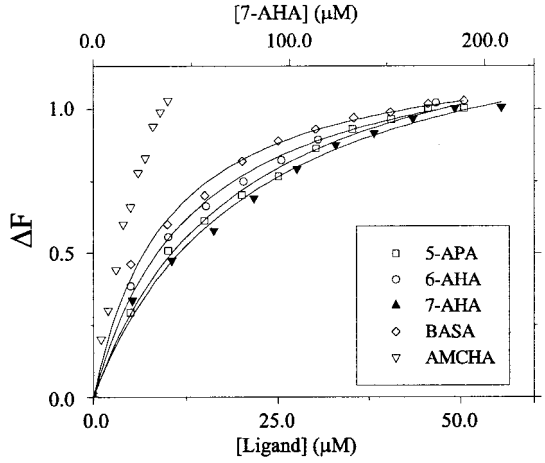

FIGURE 4: Ligand titration profiles of rNK1 with 5-APA, 6-AHA, 7-AHA, AMCHA, and BASA. ΔF denotes the change in intrinsic fluorescence at 340 nm (excitation at 296 nm). Data recorded in 50 mM phosphate buffer, pH 8, at 25 °C.

Table 1: Ligand Binding Affinities of rK1 and rNK1

ligand	K_a (mM^{-1}) rK1[a]	rNK1[b]
5-APA	44.6 ± 7	51.8 ± 3.3
6-AHA	74.2 ± 8	73.7 ± 7.0
7-AHA	13.8 ± 4.1	12.4 ± 1.1
BASA	82 ± 6	100.4 ± 7.7
AMCHA	>300[c]	227.3 ± 18.1
L-Lys	4.4 ± 0.1[d]	wb[e]
CB-NTP	4.6 ± 0.7[f]	nm[g]

[a] Determined by NMR (*14*). [b] Determined by fluorescence. [c] Value is an estimate of lower bound (*14, 40*). [d] From ref (*40*). [e] Weak binding, K_a < 5.9 mM^{-1}. [f] From ref (*51*). [g] Not measured.

227.3 ± 18.1 mM^{-1} for AMCHA. Among the linear ligands examined, 6-AHA exhibits the highest binding affinity for rNK1, in line with K_a values determined via ^{1}H NMR titrations of rK1 (Table 1) (*14*).

Far-UV CD Spectra of rNK1, rK1, and rN. The far-UV CD spectrum of the rNK1 construct (Figure 5) shows a negative band at ~204 nm and a positive band at ~187 nm. The CD spectrum of rK1 (Figure 5) shows a positive band

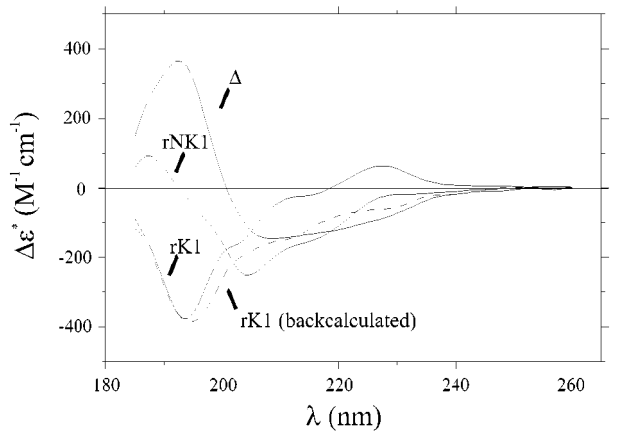

FIGURE 5: Far-UV CD spectra of rNK1 and rK1, measured (solid trace) and backcalculated (dashed trace). The Δ spectrum was obtained by subtracting rK1 from rNK1. Experimental rNK1 and rK1 spectra were recorded at 20 °C from a protein sample dissolved in 10 mM TES, 50 mM NaF, pH 7.5, to ~5 μM concentration. The simulated spectrum was constructed from the coordinates of the rK1 X-ray structure (*39*) as described under Experimental Procedures. Spectra are normalized per mole of protein.

at ~228 nm and a negative band at ~194 nm, resembling the spectra of Pgn rK2 (*35*), K4 (*36*), and the HGF rK1 (*37*). The band at ~228 nm can be attributed to contributions of aromatic and sulfur-containing amino acid side chains (*38*) and the presence of 3_1 helix (*35*). To test for the influence of aromatic and sulfur-containing side chains, the CD spectrum of rK1 was backcalculated starting from the secondary structure obtained from the X-ray crystallographic structure (*39*), as described under Experimental Procedures. The corresponding simulated curve (Figure 5) clearly shows the characteristic negative band at ~194 nm, but the positive band from 220 to 240 nm is absent, supporting that the peptide backbone conformation is unlikely to be entirely responsible for the positive band between 220 and 240 nm.

As shown above, the K1 domain within the rNK1 (rNK1/K1) folds properly, unaffected by the contiguous N-domain. Hence, the difference spectrum (Δ), obtained by subtracting the rK1 CD from the rNK1 CD, would be expected to closely reflect the contribution of the N-domain within the two-domain rNK1 construct (rNK1/N). As illustrated in Figure 5, The Δ spectrum shows a broad negative band centered at ~208 nm and a positive band at ~193 nm, a pattern that is qualitatively similar to the CD spectrum of the HGF N-domain (*37*).

Surprisingly, under identical sample conditions, a degree of variability was observed in the CD spectra of the isolated rN-domain with two main types identified, referred to hereafter as types A and B. The type A pattern (Figure 6A, trace a) is similar to the Δ spectrum (Figure 6A, trace Δ), showing a broad negative feature at ~215 nm, as well as positive band at ~193 nm. The type B (Figure 6A, trace b) shows a negative band at ~206 nm, with a shoulder at ~227 nm and positive band at ~189 nm. It is reminiscent of the previously reported spectra of rN (Figure 6A, trace d) and rPRG-B (Figure 6A, trace e) (*12*), as well as CB-NTP (Figure 6A, trace c) (*4*).

Thermal Unfolding of rNK1, rK1, and rN. A series of rK1 spectra at temperatures ranging between 5 and 95 °C (Figure 7A) show isodichroism at 198 nm, an effect not observed for rNK1 (Figure 7C). This suggests that the melting of

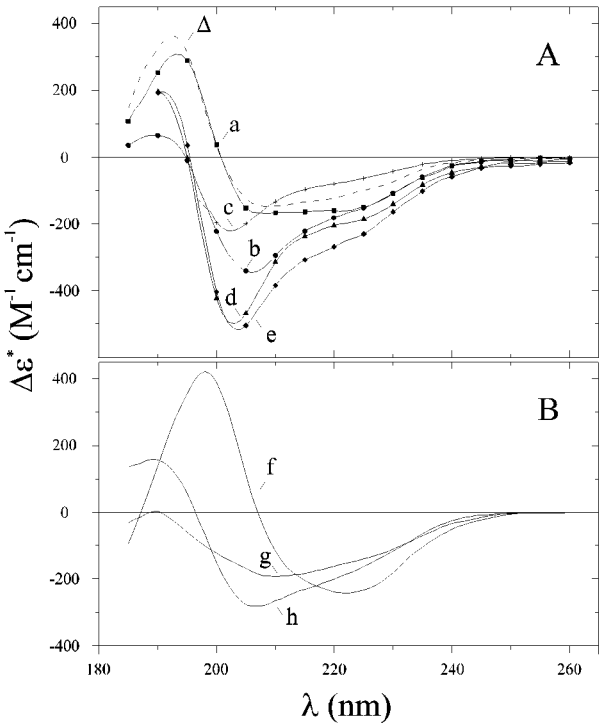

FIGURE 6: Experimental (A) and backcalculated (B) CD spectra of rN domain and related fragments. Spectra shown are rN-domain type A and type B, a and b, respectively; CB-NTP, c; rN with FXa cleavage site, d; rPRGb, e. Spectrum Δ (dashed trace) was obtained by subtracting rK1 from rNK1. Spectra a and b were recorded at the same conditions as Figure 5. Spectrum c was recorded at 5 °C in a 1 cm cell, protein concentration ~11 μM, in unbuffered water, pH 7.2. Spectra d and e were recorded at 5 °C in a 1 mm cell, protein concentration ~3 and ~7 μM, respectively, in unbuffered water, pH 7. Simulated CD spectra of HGF N-domain were computed on the basis of X-ray and NMR structures: curves f and g (two protomers, crystal) and h (solution).

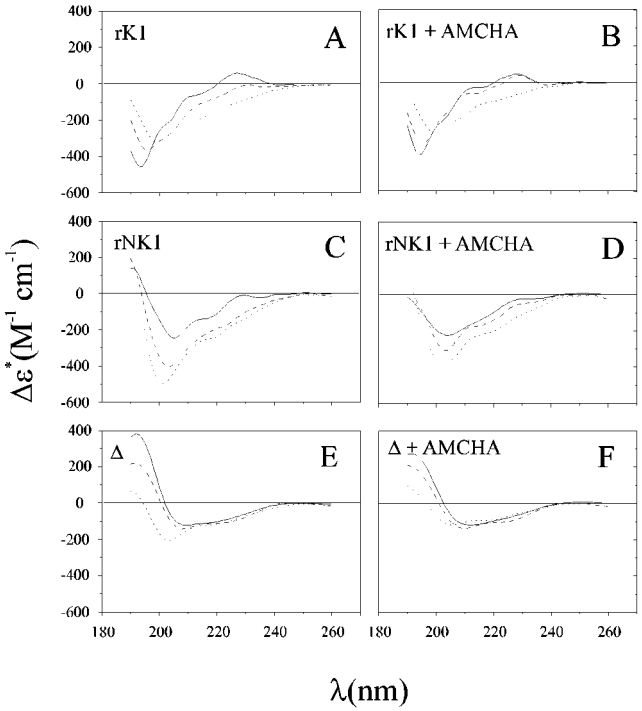

FIGURE 7: CD spectra of rK1 (A, B), rNK1 (C, D), and Δ (rNK1 minus rK1; E, F) recorded at 25 °C (solid trace), 65 °C (dashed trace), and 85 °C (dotted trace). Spectra recorded under conditions specified in the caption to Figure 5. Spectra are normalized per mole of protein.

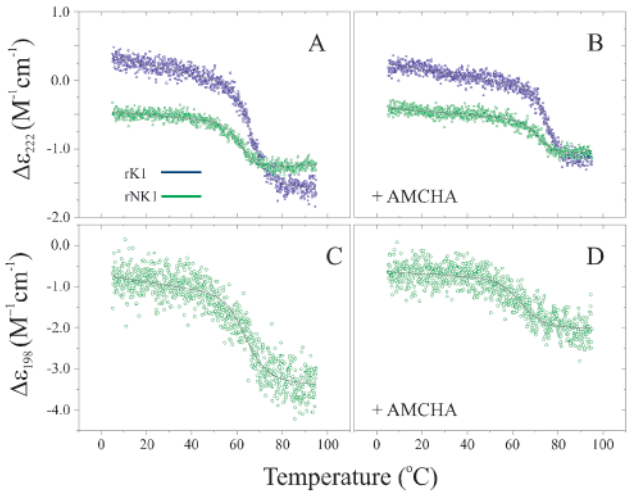

FIGURE 8: Thermal unfolding profile for rK1 domain (blue dots) and rNK1 (green dots) ligand free (A, C) and in the presence of a 5-fold excess of AMCHA (B, D). Data recorded via CD at 222 nm (A, B) and 198 nm (C, D) and shown normalized per residue. Black curve represents a nonlinear least-squares fit to eq 1 (see Experimental Procedures). Data recorded under same conditions as specified for Figure 5.

rNK1/K1 has minimal direct influence on the temperature-dependent CD of rNK1 at $\lambda = 198$ nm. Thus, taking advantage of this isodichroic point, the ΔH^{vH}, ΔS^{vH}, and T_m of rNK1/N could be determined from the rNK1 thermal unfolding profile via $\Delta\epsilon_{198}$. Likewise, minimal changes in the CD at $\lambda = 222$ nm for a series of Δ spectra between 5 and 95 °C (Figure 7E) indicate that the unfolding of rNK1/N only marginally affects the temperature-dependent dichroism at 222 nm, suggesting that the thermal unfolding of rNK1/K1 can be assessed via the temperature dependence of rNK1 at $\lambda = 222$ nm.

From the thermal unfolding of rNK1 via CD at $\Delta\epsilon_{222}$, we estimate $T_m = 62.1 \pm 0.5$ °C, $\Delta H^{vH} = 260 \pm 7$ kJ mol^{-1}, and $\Delta S^{vH} = 777 \pm 20$ J mol^{-1} K^{-1} for the rNK1/K1 (Figure 8A). By comparison, rK1 yields $T_m = 66.4 \pm 0.2$ °C, $\Delta H^{vH} = 314 \pm 6$ kJ mol^{-1}, and $\Delta S^{vH} = 924 \pm 18$ J mol^{-1} K^{-1} (Figure 8A). Consistently, the CD of rN at $\lambda = 222$ nm did not exhibit detectable temperature dependence (data not shown). In the presence of a 5-fold excess of the high-affinity kringle-specific ligand AMCHA, the T_m for rNK1/K1 increased to 72.6 ± 0.3 °C, while ΔH^{vH} slightly deceased to 250 ± 4 kJ mol^{-1} and ΔS^{vH} to 722 ± 12 J mol^{-1} K^{-1} (Figure 8B). For rK1, the 5-fold excess of AMCHA increased T_m to 75.3 ± 0.2 °C, ΔH^{vH} to 350 ± 5 kJ mol^{-1}, and ΔS^{vH} to 1004 ± 14 J mol^{-1} K^{-1} (Figure 8B).

It is interesting that upon AMCHA addition, the CD of the Δ spectrum does not significantly change (Figure 7B,D,F), revealing that the N-module within rNK1 is impervious to events within the kringle domain. For rNK1/N, in both the absence and the presence of a 5-fold excess of AMCHA, the temperature dependence of $\Delta\epsilon_{198}$ yields $\Delta H^{vH} = 206 \pm 13$ and 190 ± 19 kJ mol^{-1}, $\Delta S^{vH} = 610 \pm 38$ and 565 ± 61 J mol^{-1} K^{-1}, respectively, while T_m remained constant at ~64 °C (Figure 8C,D). Consistently, rK1 exhibited no temperature-dependent melting at $\Delta\epsilon_{198}$ (data not shown). Unfortunately, despite evidence of temperature-induced unfolding, it was not possible to accurately

measure ΔH^{vH} and ΔS^{vH} for the thermal unfolding of rN via $\Delta\epsilon_{198}$ owing to poor sensitivity, a result of its low solubility (data not shown).

DISCUSSION

Ligand Binding to rNK1. Vis-à-vis the reported K_a values for rK1 (*14*), the ligand binding affinities for rNK1 (Table 1) indicate that the N-domain does not significantly interfere with the binding of these ligands to rNK1/K1. An apparent exception may be the interaction with L-lysine, which is known to exhibit only weak binding to the isolated K1 (*40*), comparable to that of CB-NTP (*4*), namely, $K_a \sim 4.5\ mM^{-1}$. Thus, it is conceivable that weak *intermolecular* interactions between the N and K1 domains of rNK1 modulate the affinity of the rNK1/K1 for L-lysine, leading to erratic results, with the derived K_a values ranging between 0.7 and 5.9 mM^{-1}.

Structural Characterization of rNK1, rK1, and rN. The analysis of the rNK1 CD (Figure 5) via CDsstr (*28*) yields 2% α-helix, 25% *β*-sheet, 12% *β*-turns, 3% 3_{10}-helix, 11% 3_1-helix, and 45% "other". For rK1 (Figure 5), we obtain ~0% α-helix, 24% *β*-sheet, 11% *β*-turns, 1% 3_{10}-helix, 12% 3_1-helix, and 51% other, which closely agree with those values estimated from the X-ray crystallographic structure (*39*) using the program xtlsstr (*32*): 4% α-helix, 14% *β*-sheet, 24% *β*-turns, 0% 3_{10}-helix, 8% 3_1-helix, and 51% other. The differences can be attributed to effects from aromatic and sulfur-containing side chains as discussed above.

The secondary structure content (Table 2) estimated from the rN type A CD spectrum (Figure 6, trace a) yields 15% α-helix, 20% *β*-sheet, 10% *β*-turns, 6% 3_{10}-helix, 8% 3_1-helix, and 40% other, while for the type B spectrum (Figure 6, trace b) we obtain 8% α-helix, 16% *β*-sheet, 11% *β*-turns, 5% 3_{10}-helix, 5% 3_1-helix, and 56% other. These estimates indicate that the type A spectrum stems from a somewhat more ordered conformation than the type B spectrum. The Δ spectrum (Figure 6, trace Δ), which resembles the type A spectrum, yields 10% α-helix, 25% *β*-sheet, 11% *β*-turns, 6% 3_{10}-helix, 8% 3_1-helix, and 39% other, results similar to the estimates of the type A spectrum, as expected. Moreover, adding the secondary structure from the Δ and rK1 spectra reproduces the secondary structure estimates from the rNK1 CD, consistent with the assumption that both rK1 and the Δ spectra reflect rNK1/K1 and rNK1/N, respectively. The type B spectrum (Figure 6, trace b), the CB-NTP (*4*) (Figure 6, trace c), the previously recorded spectra of rN (*12*) (Figure 6, trace d) and rPRG-B (*12*) (Figure 6, trace e) all show a negative band of variable intensity at ~205 nm. Secondary structure estimates based on these spectra (Table 2) reflect relatively less ordered forms than the ones responsible for the type A or Δ spectra.

Recently, coordinates of the HGF N-domain NMR solution and HGF NK1 X-ray crystallographic structures have become public (*41*−*43*). In the NK1 crystal, the unit cell contains a head-to-tail dimer with the N-terminal domain of one protomer facing the kringle domain of the other. Motivated by the variability we observe for the CD spectra of the Pgn rN variants (Figure 6A), the secondary structure content of the HGF NK1/N domain was calculated (Table 2) as described above for Pgn K1, starting from the coordinates of the HGF NK1/N (*42*) for each of the two protomers. On this basis, the far-UV CD spectrum was backcalculated for each HGF NK1/N within the unit crystal (*42*) as well as for the isolated HGF N-domain in solution (*41*). It is revealing that these simulated spectra (Figure 6B) exhibit features that qualitatively agree with the measured spectra for the Pgn rN (Figure 6A). The Δ spectrum and the type A spectrum (Figure 6A, trace Δ, a), which reflect the more defined conformation of the Pgn N-domain, resemble a mix of the CD spectra calculated from the crystallographic structure of the HGF NK1/N (Figure 6B, traces f and g). In contrast, the rN type B spectrum (Figure 6, trace b), which stems from a less defined conformation, resembles the curve calculated from the NMR solution structure HGF N-domain (Figure 6, trace h). Overall, the subtle differences between the various reported HGF N-domain structures are in line with the variability in their predicted (Figure 6B, traces f, g, and h) and experimental (*37*) CD signatures. Likewise, the range of rN spectra suggests a similar degree of conformational plasticity for the Pgn N-domain.

Table 2: Secondary Structure of the Pgn N-Domain and Homologous Modules

protein	fragment	α-helix	*β*-sheet	*β*-turn	3_{10}-helix	3_1-helix	other
Pgn[a]	Δ	10	25	11	6	8	39
	rN (type A)	15	20	10	6	8	40
	CB-NTP[b]	6	8	8	4	5	67
	rN (type B)	8	16	11	5	5	56
	rN[c]	16	4	15	10	5	50
	rPRG-B[c]	19	6	16	10	4	45
HGF[d]	N[e]	12	13	15	7	4	50
	NK1/N (1)[f]	14	29	12	4	3	38
	NK1/N (2)[f]	8	15	16	3	7	51

[a] Secondary structure from CD spectra (Figure 6). [b] From ref (*4*). [c] From ref (*12*). [d] Secondary structure calculated from X-ray crystal and NMR solution structures. [e] From ref (*41*). [f] From ref (*42*).

Thermal Stability of rNK1, rK1, and rN. For rK1, a $\Delta H^{vH} = 314\ kJ\ mol^{-1}$ was estimated from the CD thermal melting profile (Figure 8A, Table 3). The differences between this value and the measured calorimetric ΔH of 243 kJ mol^{-1} (*13*) likely stem from the diverse experimental conditions compounded by the known variability between equililbrium van't Hoff and direct, calorimetric heat capacity analyses. On the other hand, there is agreement between the T_m measured in this study, 66.4 °C, and that measured via DSC of 67.7 °C (*13*).

In a 5-fold excess of the ligand AMCHA, the T_m of both rK1 and rNK1/K1 increased ~10 °C. This is in line with calorimetric (*13*, *44*−*47*) and NMR (*48*) studies on various kringles which show that saturation with the lysine-type ligand 6-AHA increases T_m by ~10−20 °C.

Comparison of T_m values (Table 3) reveals that NK1/K1 is less thermally stable than rK1 in isolation, whether in the presence or in the absence of ligand. This result suggests that the attached N-domain destabilizes the K1 domain against thermal unfolding. Such a negative cooperativity between adjacent domains has been observed before in Pgn: on the basis of DSC experiments, Privalov and coworkers (*45*) have suggested that K1 is thermodynamically more stable as an isolated unit than within the K123

Table 3: Thermodynamic Parameters for Unfolding of rK1 and rNK1[a]

	N-domain			K1 domain		
construct	T_m	ΔH^{vH}	ΔS^{vH}	T_m	ΔH^{vH}	ΔS^{vH}
rK1				66.4 ± 0.2	314 ± 6	924 ± 18
rK1 + AMCHA				75.3 ± 0.2	350 ± 5	1004 ± 14
rNK1	64.0 ± 0.2	206 ± 13	610 ± 38	62.1 ± 0.5	260 ± 7	777 ± 20
rNK1 + AMCHA	64.1 ± 0.5	190 ± 19	565 ± 61	72.6 ± 0.3	250 ± 4	722 ± 12

[a] Determined from CD intensity at 198 nm (N) and 222 nm (K). Units are °C for melting temperatures (T_m), kJ mol^{-1} for enthalpies (ΔH^{vH}), and J mol^{-1} K^{-1} for entropies (ΔS^{vH}).

construct, and more recently Misselwitz et al. (*49*) concluded that K5 destabilizes the C-terminal serine protease. This may be a characteristic of multimodular proteins at large, where the isotropic translation/rotation motions of the various autonomous globular domains only loosely couple to each other, resulting in Brownian push−pull interactions of one domain against the other that could contribute a bias toward structural unfolding via stretching of the flexible linking peptides.

In contrast to the results measured for rK1 and rNK1/K1 from thermal unfolding via $\Delta\epsilon_{222}$, thermal unfolding monitored via $\Delta\epsilon_{198}$ probes the thermal stability of the N-domain. Consistent with domain independence, a 5-fold excess of AMCHA, while binding to the rNK1/K1, did not significantly affect the T_m or ΔH^{vH} of rNK1/N. Furthermore, differences between ΔH^{vH} measured via $\Delta\epsilon_{198}$ from ΔH^{vH} measured via $\Delta\epsilon_{222}$ indicate that rNK1/N is more pliable than rNK1/K1.

CONCLUSIONS

In practice, a DSC thermogram of the rNK1 construct in the absence of ligand would result in a single observable transition, as the T_m values for the two domains differ by only 2.1 °C. Thus, to resolve the calorimetric enthalpies and melting temperatures for each subunit, the thermogram would have to be mathematically deconvolved (*50*). As we show in this paper, one may take advantage of CD spectroscopy to untangle calorimetrically coincident thermal transitions into its components. This is a potentially useful approach for physically characterizing multidomain constructs composed of different modules.

The CD-monitored thermal melting experiments verify that both rNK1/N and rNK1/K1 are folded at ambient temperatures (Figure 8A,C and Table 3). Moreover, affinity chromatography on a lysine-conjugated gel (Figure 2B), the 1D ^{1}H NMR spectrum (Figure 3), and ligand titration experiments, which show that rNK1/K1 binds lysyl-type ligands with affinities comparable to isolated K1 (Figure 4 and Table 1) (*14*), confirm that rNK1/K1 adopts the proper kringle conformation. Ligand saturation with AMCHA (Figure 8B,D), which stabilizes the K1 domain against thermal unfolding while showing no effect on the N-domain, demonstrates the independence between the two modules in the NK1 construct. ESI-MS and N-terminal sequence analysis of rNK1 indicate that the hinge region between the N and K1 domains is exposed as it is accessible to EK and prone to cleavages under mild acidic conditions, suggesting lability for the interdomain link peptide. It is interesting that the adjacent rNK1/N tends to thermally destabilize the K1 domain in both the presence and the absence of ligand. However, in the two-domain construct, rNK1/N adopts the more ordered type A conformation (Figure 6), suggesting that an intact linking peptide helps drive rNK1/N to its "native" folding at the expense of destabilizing the neighboring rNK1/K1. On the other hand, by itself the isolated rN domain exhibits a variable CD signature (Figure 6A), consistent with the reported observations (*12*) that this domain is susceptible to FXa digestion and exhibits fast ^{1}H-^{2}H exchange in solution which, when combined with the characteristics of the ^{1}H NMR spectrum (*12*), indicate a rather loosely structured fold. The three reported structures of HGF N-domain indicate that this domain may also be endowed with a somewhat flexible structure which seems to adjust to the environmental conditions, such as aqueous solution (*41*) or crystal lattice (*42*, *43*). Revealingly, the simulated CD traces of the three structures qualitatively recall the variable patterns of the Pgn N-domain CD spectra (Figure 6).

From the combined evidence, we are led to propose that the NMR (*41*) and crystallographic (*42*, *43*) structures of the HGF N-terminal domain, while valuable to envision the folding characteristics of the PAN motif, should be interpreted with some caution in the context of Pgn N-domain function. Our results lead us to suggest that the structural plasticity we observe may be of functional significance in order to facilitate the N-domain to interact intramolecularly, presumably with kringles (*3*, *4*, *51*), as a structural switch that drives Pgn from its open to its close conformation (*1*, *5*, *6*).

ACKNOWLEDGMENT

We thank Mr. U. Kämpfer for expert technical assistance and Dr. D. Marti for the ^{1}H NMR spectrum of rK1.

REFERENCES

1. Sjöholm, I., Wiman, B., and Wallén, P. (1973) *Eur. J. Biochem. 39*, 471−479.
2. Markus, G. (1996) *Fibrinolysis 10*, 75−85.
3. Ramesh, V., Rajan, N., Laursen, R. A., and Llinás, M. (1995) *Blood Coagulation Fibrinolysis 6*, 207−218.
4. An, S. S., Marti, D. N., Carreño, C., Albericio, F., Schaller, J., and Llinás, M. (1998) *Protein Sci. 7*, 1947−1959.
5. Mangel, W. F., Lin, B. H., and Ramakrishnan, V. (1990) *Science 248*, 69−73.
6. Ponting, C. P., Marshall, J. M., and Cederholm-Williams, S. A. (1992) *Blood Coagulation Fibrinolysis 3*, 605−614.
7. Nakamura, T., Nishizawa, T., Hagiya, M., Seki, T., Shimonishi, M., Sugimura, A., Tashiro, K., and Shimizu, S. (1989) *Nature 342*, 440−443.
8. Skeel, A., Yoshimura, T., Showalter, S. D., Tanaka, S., Appella, E., and Leonard, E. J. (1991) *J. Exp. Med. 173*, 1227−1234.
9. Ichinose, A. (1992) *Biochemistry 31*, 3113−3118.
10. Tordai, H., Bányai, L., and Patthy, L. (1999) *FEBS Lett. 461*, 63−67.

11. Weissbach, L., and Treadwell, B. V. (1992) *Biochem. Biophys. Res. Commun. 186*, 1108−1114.
12. Lewis, V. O., Gehrmann, M., Weissbach, L., Hyman, J. E., Rielly, A., Jones, D. G., Llinás, M., and Schaller, J. (1999) *Eur. J. Biochem. 259*, 618−625.
13. Menhart, N., Sehl, L. C., Kelley, R. F., and Castellino, F. J. (1991) *Biochemistry 30*, 1948−1957.
14. Marti, D. N., Hu, C. K., An, S. S., von Haller, P., Schaller, J., and Llinás, M. (1997) *Biochemistry 36*, 11591−11604.
15. Brunisholz, R., Lerch, P. G., and Rickli, E. E. (1979) in *Haemostasis and thrombosis* (Neri Serneri, G. G., Ed.) pp 757−761, Academic Press, London.
16. Hochuli, E., Bannwarth, W., Döbeli, H., Gentz, R., and Stüber, D. (1988) *Biotechnology 213*, 1321−1325.
17. Forsgren, M., Råden, B., Israelsson, M., Larsson, K., and Hedén, L. O. (1987) *FEBS Lett. 213*, 254−260.
18. Cleary, S., Mulkerrin, M. G., and Kelley, R. F. (1989) *Biochemistry 28*, 1884−1891.
19. Marti, D., Schaller, J., Ochensberger, B., and Rickli, E. E. (1994) *Eur. J. Biochem. 219*, 455−462.
20. Söhndel, S., Hu, C. K., Marti, D., Affolter, M., Schaller, J., Llinás, M., and Rickli, E. E. (1996) *Biochemistry 35*, 2357−2364.
21. Fontana, A. (1972) *Methods Enzymol. 25*, 419−423.
22. Chang, J. Y., and Knecht, R. (1991) *Anal. Biochem. 197*, 52−58.
23. Bidlingmeyer, B. A., Cohen, S. A., and Tarvin, T. L. (1984) *J. Chromatogr. 336*, 93−104.
24. Press, W. H., Flannery, B. P., Teukolsky, S. A., and Vetterling, W. T. (1989) *Numerical Recipes*, Cambridge University Press, Cambridge, U.K.
25. Johnson, W. C. (1990) *Proteins: Struct., Funct., Genet. 7*, 205−214.
26. Copeland, R. A. (1994) *Method for protein analysis. a practical guide to laboratory protocols*, Chapman & Hall, New York.
27. Pace, C. N., Vajdos, F., Fee, L., Grimsley, G., and Gray, T. (1995) *Protein Sci. 4*, 2411−2423.
28. Johnson, W. C. (1999) *Proteins: Struct., Funct., Genet. 35*, 307−312.
29. Venyaminov, S., Baikalov, I. A., Shen, Z. M., Wu, C. S., and Yang, J. T. (1993) *Anal. Biochem. 214*, 17−24.
30. Sreerama, N., Venyaminov, S. Y., and Woody, R. W. (2000) *Anal. Biochem. 287*, 243−251.
31. Yadav, S., and Ahmad, F. (2000) *Anal. Biochem. 283*, 207−213.
32. King, S. M., and Johnson, W. C. (1999) *Proteins: Struct., Funct., Genet. 35*, 313−320.
33. Miyashita, C., Wenzel, E., and Heiden, M. (1988) *Haemostasis 18 (Suppl. 1)*, 7−13.
34. Rejante, M. R., and Llinás, M. (1994) *Eur. J. Biochem. 221*, 939−949.
35. Marti, D. N., Schaller, J., and Llinás, M. (1999) *Biochemistry 38*, 15741−15755.
36. Castellino, F. J., de Serrano, V. S., Powell, J. R., Johnson, W. R., and Beals, J. M. (1986) *Arch. Biochem. Biophys. 247*, 312−320.
37. Stahl, S. J., Wingfield, P. T., Kaufman, J. D., Pannell, L. K., Cioce, V., Sakata, H., Taylor, W. G., Rubin, J. S., and Bottaro, D. P. (1997) *Biochem. J. 326*, 763−772.
38. Krittanai, C., and Johnson, W. C. (1997) *Anal. Biochem. 253*, 57−64.
39. Mathews, I. I., Vanderhoff-Hanaver, P., Castellino, F. J., and Tulinsky, A. (1996) *Biochemistry 35*, 2567−2576.
40. Rejante, M. R. (1992) *Proton NMR studies on the structure and ligand-binding properties of human plasminogen kringles 1 and 4.*, Ph.D. dissertation, Carnegie Mellon University, Pittsburgh, PA.
41. Zhou, H., Mazzulla, M. J., Kaufman, J. D., Stahl, S. J., Wingfield, P. T., Rubin, J. S., Bottaro, D. P., and Byrd, R. A. (1998) *Structure 6*, 109−116.
42. Ultsch, M., Lokker, N. A., Godowski, P. J., and de Vos, A. M. (1998) *Structure 6*, 1383−1393.
43. Chirgadze, D. Y., Hepple, J. P., Zhou, H., Byrd, R. A., Blundell, T. L., and Gherardi, E. (1999) *Nat. Struct. Biol. 6*, 72−79.
44. Castellino, F. J., Ploplis, V. A., Powell, J. R., and Strickland, D. K. (1981) *J. Biol. Chem. 256*, 4778−4782.
45. Novokhatny, V. V., Kudinov, S. A., and Privalov, P. L. (1984) *J. Mol. Biol. 179*, 215−232.
46. Chang, Y., Mochalkin, I., McCance, S. G., Cheng, B., Tulinsky, A., and Castellino, F. J. (1998) *Biochemistry 37*, 3258−3271.
47. Nilsen, S. L., Prorok, M., and Castellino, F. J. (1999) *J. Biol. Chem. 274*, 22380−22386.
48. De Marco, A., Motta, A., Llinás, M., and Laursen, R. A. (1985) *Biophys. J. 48*, 411−422.
49. Misselwitz, R., Welfle, K., and Welfle, H. (1994) *Int. J. Biol. Macromol. 16*, 187−194.
50. Privalov, P. L., and Potekhin, S. A. (1986) *Methods Enzymol. 131*, 4−51.
51. An, S. S., Carreño, C., Marti, D. N., Schaller, J., Albericio, F., and Llinás, M. (1998) *Protein Sci. 7*, 1960−1969.

BI016018J